Experimental Measurement of the Dynamics of Foil Targets under the Impact of Intense Pulses of Soft X Radiation

J. Edwards,* M. Dunne, R. Taylor, and O. Willi
Blackett Laboratory, Imperial College of Science Technology and Medicine, London SW7 2BZ, United Kingdom

C. A. Back†
Laboratoire PMI, Ecole Polytechnique, Palaiseau, CEDEX, France

S. J. Rose
Rutherford Appleton Laboratory, Chilton, Didcot, Oxon. OX11 0QX, United Kingdom
(Received 26 August 1992; revised manuscript received 11 June 1993)

The dynamics of plastic foils of different thicknesses which were irradiated with intense, approximately Planckian soft-x-ray pulses, have been investigated using a high magnification (80×), time-resolving extreme ultraviolet (95 or 205 eV) imaging technique for the first time. The experimental results are discussed and compared with hydrocode simulations.

PACS numbers: 52.50.Jm, 52.25.Jm, 52.25.Nr

The interaction of intense, ionizing radiation fields with matter is of fundamental interest and is responsible for a host of natural, astrophysical phenomena, perhaps even triggering of the gravitational collapse of gas clouds leading to stellar formation. Recently, considerable interest in the generation of intense radiation fields in the laboratory has resulted from the possibility of using these as drivers for inertial confinement fusion (ICF) as well as for more fundamental studies. Several studies of target heating and acceleration by laser light have been made [1]. More recently, several experimental studies using x-ray heating have been reported [2,3]. However, only limited information on the dynamics of x-ray heated targets has become available [4]. Here we report the first time resolved measurements of the dynamics of thin foil targets of different thicknesses, which were irradiated with intense, approximately Planckian soft-x-ray pulses and diagnosed using a high magnification (80×) time-resolving (100 ps), high resolution, extreme ultraviolet (XUV) imaging technique. This technique has advantages over other methods for diagnosing target dynamics because of its high magnification and spatial resolution. Also, the method allows experiments to access plasma regions previously inaccessible to both harder x-ray (keV) and visible (eV) techniques by allowing diagnosis of radiation at any photon energy up to the limit of the multilayer technology used for the image device (400–500 eV). The experimental results are compared to simulated data generated by performing detailed ray-trace calculations on radiation-hydrocode modeling results.

The experiments were carried out on the Nd:glass laser, VULCAN, of the Central Laser Facility at the Rutherford Appleton Laboratory. Targets consisted of stripes of plastic (CH, parylene, or $C_{10}O_4H_8$, Mylar), 500 μm wide and up to 6 μm thick. These were irradiated with a soft-x-ray pulse of 1.2 ns (FWHM) duration, emitted from the rear of a laser-irradiated "burnthrough" foil [5,6]. The burnthrough foil consisted of 75 nm of gold (Au) supported on 1 μm of CH and was positioned parallel to the sample target and separated from it by approximately 650 μm. The laser energy was delivered into a 750 μm focal spot on the burnthrough target through $f/10$ lenses by up to five separate beams arranged in the VULCAN cluster configuration (13 degree cone angle). Random-phase plates were used to reduce large scale nonuniformities over the focal spot. Laser irradiances of up to 10^{14} W cm^{-2} were used. The soft-x-ray flux and pulse shape emitted from the rear of the burnthrough foil was measured using a time-resolving photodiode and diamond photoconductive detectors (PCD) operated in time-integrating mode. The PCDs were calibrated against the DANTE filtered photodiode array in burnthrough foil characterization experiments on the NOVA laser at the Lawrence Livermore Laboratory prior to use in the experiments reported here [6]. Allowing for experimental uncertainties and spatial and angular variations in the emitted radiation, it is estimated that the peak soft-x-ray flux at the surface of the plastic sample foils was between 1.25×10^{12} W cm^{-2} and 2.5×10^{12} W cm^{-2}. The heated targets were probed side-on by a quasicontinuum soft-x-ray pulse of similar duration to the driving pulse. The probe (backlighter) pulse was provided by irradiating a 500 μm diam Au wire with around 10 J of green laser light. The backlighter was positioned in a plane parallel to the target surfaces and at a distance from the target of approximately 3 mm. The backlighter emission was timed to probe the stripe target 250 ps before the main soft-x-ray pulse was incident, to record the initial position of the target. A narrow spectral band (~5–10 Å) of the backlighter radiation at the stripe was selectively imaged (together with any plasma self-emission) onto the slit (oriented perpendicular to the target surface) of an x-ray streak camera with a magnification of approximately 80× using a spherical multilayer mirror. Two different mirror coatings were used to record images at either 130 Å (95 eV) or 60 Å (205 eV). The two different wave-

0031-9007/93/71(21)/3477(4)$06.00

lengths allow different regions of the plasma to be probed since the transmission of probe radiation through a path-length L of plasma along which the density is ρ and the opacity κ is given by $\exp(-\rho\kappa L)$ where κ is a strong function of photon energy. The temporal resolution of the instrument was approximately 100 ps while the spatial resolution depends both on the target and the F number of the system. For the setup used here, detailed ray traces of the imaging system indicated a spatial resolution at the rear of the targets of slightly less than 1 μm. The actual spatial resolution achieved was around 4–5 μm as determined by the measured rear edge width of an unheated foil. Degradation of the intrinsic resolution results partly from the streak camera spatial resolution (equivalent to about 2 μm in the target plane), target uniformity, and small errors in focusing. The imaging technique is described in detail elsewhere [7].

Figure 1 shows streak records in the (t,z) plane (t = time, z = position measured perpendicular to the target surface) obtained at probe wavelengths of 60 and 130 Å for x-ray heated CH foils, initially 2.8 μm thick. In both cases, the x-ray irradiance at the targets was approximately the same (1.25–2.5×10^{12} W cm^{-2}) so that the plasmas generated were very similar. At first, the foil appears as a dark shadow because it is initially opaque to the probe radiation. When the soft-x-ray pulse turns on, plasma can be seen to ablate from the surface of the target and expand into the vacuum. At the same time, a shock wave is driven into the stripe by the pressure exerted by the ablating plasma. A short time later, after the shock wave has passed through the foil, the rear of the target can be seen to accelerate to the left, driven partly by the ablation pressure. Also, significant nearly uniform (volumetric) heating of the foil occurs because a significant fraction of the drive energy exists in the spectral region just below the cold carbon K edge (around 260 eV), where photon mfps are of the order of the target thickness even in cold material. The volumetric heating causes the foil to behave explosively leading to foil decompression and contributing to the motion of the rear of the target. Further heating of the target reduces its opacity allowing more of the drive spectrum to contribute to global heating, accentuating the explosive behavior.

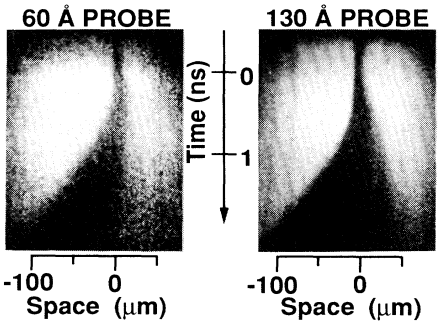

FIG. 1. Streaked radiograms of 2.8 μm CH foils heated by soft x rays for probe wavelengths of 130 and 60 Å. Drive incident from right.

Microdensitometry of the data in Fig. 1 shows the half-height intensity contours at the rear of the targets to follow very similar trajectories for the two probe wavelengths. This is consistent with the large density gradient that would be expected at the rear of the foil. On the other hand, the different plasma regions that the two different wavelengths probe are easily resolvable in the front plasma.

The soft-x-ray-target interaction was simulated using the 1D Lagrangian hydrodynamics code, MEDUSA, coupled to a 1D multigroup radiation transport code which assumes local thermodynamic equilibrium [8,9]. The measured temporal evolution of the soft-x-ray pulse was used in the calculations. Simulations were performed with peak x-ray fluxes emitted from the rear surface of the burnthrough foil of 5×10^{12} (low flux) and 1×10^{13} W cm^{-2} (high flux), which bracket the experimental conditions. The spectral form of the radiation was assumed to be that of a 100 eV Planckian, scaled in magnitude to give the required flux. Opacities were calculated from tabulated values generated by the detailed opacity code, IMP [10].

The simulation results were compared with the experimental data by generating probe transmission contours in the (t,z) plane from the predicted plasma density and temperature profiles using a ray trace of the experimental system. Opacities were taken from the same grid used in the hydrocode calculations. The plasma flow was assumed to be one-dimensional so that the plasma width was constant at the initial target width, 500 μm. An exact assessment of the accuracy of this assumption is difficult without 2D simulations. However, the approximation is expected to be reasonably good during most of the observation time for these experiments since the target moves only tens of microns compared to the 500 μm initial foil width. The predicted and measured half-height intensity contours for both wavelengths are shown in Fig. 2. The high-flux prediction of the 60 Å probe image is not plotted beyond around 1.5 ns because the front and rear surface contours join together shortly after. The suitability of significantly shorter wavelength (higher energy) probe radiation for diagnosing these foils was assessed by predicting radiograms of the targets for 4 Å probe radiation and perfect instrumental spatial resolution. It was found that these targets became transparent to the probe radiation after around 0.8–1 ns. During this time the foil was predicted to appear no more than 10 μm wide and the half-height contour was predicted to move no more than around 15 μm, both of which are close to the spatial resolution limit of the APC technique. These figures were quite insensitive to the drive flux used in the simulations, which is clearly not the case for the probe wavelengths used here and indicates the obvious advan-

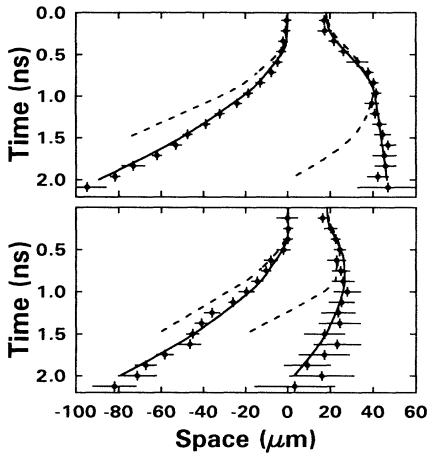

FIG. 2. Half-height intensity contours for 130 Å probe (upper plot) and 60 Å probe (lower plot) taken from the data shown in Fig. 1. Hydrocode predictions are shown for x-ray drive fluxes of 1.25×10^{12} W cm^{-2} (solid line) and 2.5×10^{12} W cm^{-2} (dashed line). Experimental error bars include uncertainties due to any initial target tilt and/or structure in the photocathode (detector).

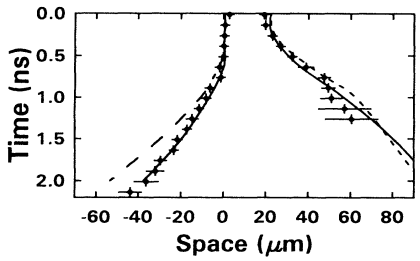

FIG. 3. Half-height probe intensity contours for an x-ray driven 6 μm Mylar foil and hydrocode predictions for x-ray drive fluxes of 1.25×10^{12} W cm^{-2} (solid line) and 2.5×10^{12} W cm^{-2} (dashed line). Error bars include uncertainties due to any initial target tilt and/or structure in the photocathode (detector).

tage of the use of longer wavelength probe radiation for these types of targets.

The front and rear plasma profiles are predicted to be sensitive to the driving x-ray flux and the experimental data is well represented by the low flux prediction in both cases. The half-height intensity contours at the rear of the target are predicted to be almost identical in (t,z) for both wavelengths at least up to around 1.2 and 1.5 ns, for the higher and lower fluxes, respectively. In fact, it was predicted that the transmission contours (in the range 0.0–1.0) of all possible probe wavelengths between 8 and 195 Å (1500 and 65 eV) followed roughly the same trajectory and remained tightly bunched at least for the first ~1 ns of the simulation. This implies that the accuracy of the opacity calculations is not critical in forming the transmission contours at the rear of the target during this time. On the other hand, the front side profiles are clearly very sensitive to the probe wavelength used. This is because in this case the radiative opacity is mainly due to bound-free transitions involving carbon L-shell electrons, the average number of which is very sensitive to the plasma temperature, in particular, and density. The opacity at a probe wavelength of 60 Å is smaller than that at 130 Å at all times for these experiments. Consequently, because the plasma density and radiative opacity increase towards the target surface, the cutoff for the 60 Å probe occurs closer to the initial target surface than that for the 130 Å probe.

The high flux prediction for the 60 Å probe indicates that the whole foil becomes largely transparent to the probe radiation after about 1.5–1.6 ns. From examining the radiative opacity of the plasma for the temperatures that might be expected for these drive conditions, the peak density in the foil at this time must be around 0.03 g/cm^3, i.e., a decompression of around 30×. In fact, the peak density at 1.5 ns is predicted to be 0.027 g/cm^3 for the high flux simulation and 0.046 g/cm^3 for the low flux simulation. The target decompression leads to the development of a velocity gradient in the accelerated (unablated) region of the foil. In this case, the velocities of the rear side half-height contours, close to the rear of the foils, are roughly twice the center-of-mass (c.m.) velocities of the unablated material. It is worth noting that for the case of thin foils illuminated by direct laser light at moderate irradiances, little or no decompression of the unablated region of the target results during the laser pulse [11].

For ICF applications, even small degrees of global heating (preheating) of the targets is highly undesirable since the fuel is raised to a higher adiabat thereby reducing the compression attainable for a given drive. It is not presently possible to achieve the drive fluxes that are thought to be required for fusion in the laboratory. However, in order to examine target behavior and test modeling capability in a less preheated and explosive regime, 6 μm thick Mylar foils were used in place of the 2.8 μm CH stripes. The Mylar targets are expected to behave more ablatively (and less explosively) than the pure CH foils because they are thicker, denser, and have a higher opacity to the heating x rays. The x-ray flux at the target was again between 1.25 and 2.5×10^{12} W cm^{-2} for direct comparison with the thinner foil experiments.

The experimentally measured half-height contours for a probe wavelength of 130 Å for the 6 μm foil are compared with predictions from numerical simulations in Fig. 3. The front surface measurement is only plotted for the first nanosecond due to fall off in the backlighter contrast. As in the case of the thinner foils, good agreement is found between the low flux simulation and experiment. In order to assess whether inaccuracies in the opacity modeling may be responsible for the obvious trend towards agreement between experiment and the low flux simulations, calculations were also performed for the 6

μm foil using different opacity models. Omission of the bound-bound contribution to the IMP radiative opacities in the simulations resulted in typically up to 10% changes in rear surface position, compared to the up to 50% changes resulting from a factor of 2 increase in drive flux. Consequently, it is expected that the drive obtained in the experiment was closer to the lower value used for the simulations. This may result from spatial and angular variations of the source at the rear of the burnthrough foils, and/or experimental uncertainties in the diode measurements.

From the results shown in Fig. 3, it is possible to obtain upper limits of the mean (in time) pressure, $\langle P_a \rangle$, generated by the ablation of target material ($\langle P_a \rangle \approx \rho z \langle a \rangle$, with $\langle a \rangle = v/t$, where ρ and z are the initial density and thickness of the target, respectively). These are upper limits because the accelerated region of the target loses mass into the plasma blowoff during the acceleration. Also, since the probe wavelengths used closely follow regions near the rear of the targets, the measured half-height contour velocity is larger than the c.m. velocity of the unablated region of the foil because of preheating of the target and subsequent decompression. (In general, when decompression occurs, it is not possible for a single probe wavelength to follow the trajectory of the c.m. of the accelerated region of the foil because the density and opacity are time dependent.) At $t = 1.5$ ns, when the drive power has fallen to just below one half its peak value, the experimentally measured rear half-height contour velocity is approximately $(3.1 \pm 0.2) \times 10^6$ cm s^{-1}. This leads to an estimate of the upper limit (i.e., without accounting for ablation or decompression) of the mean ablation pressure of $\langle P_a \rangle \approx 1.7$ Mbar. For comparison, the values predicted by the low and high flux simulations are 0.7 and 1 Mbar, respectively. As expected, however, the decompression is less pronounced than for the thinner CH foils; the ratio of the rear surface velocity to the c.m. value in the accelerated matter is approximately 1.5 as opposed to 2 for the thinner pure CH targets; also the peak density of the Mylar target is around one third the initial value in comparison with less than one tenth for the CH foils.

The values inferred for $\langle P_a \rangle$ above have been compared with other experimental results and (semi-) analytic models. The results presented here are found to be reasonably consistent with the previous data. For example, the pressure generated by soft-x-ray ablation has been estimated from shock velocity measurements in aluminum foil targets to be around 1.3 Mbar for an x-ray flux on target of around 2×10^{12} W cm^{-2} [12]. This value is consistent with a semianalytic model and is comparable to the results presented here [13].

In summary, using soft-x-ray probing, we have investigated the dynamics of planar foil targets of different thicknesses which were irradiated by intense, approximately Planckian soft-x-ray pulses. We find that the experimental results are reproduced well by hydrocode calculations using a low flux drive. In addition, the results are consistent both with previous shock velocity measurements and semianalytic models. For the particular experimental arrangement reported here and for peak x-ray fluxes at the target surface of $1.25\text{–}2.5 \times 10^{12}$ W cm^{-2} it was inferred that mean ablation pressures of around 1 Mbar were generated by soft-x-ray irradiation of the targets. It is worth noting that in similar experiments, where thin foils were heated with soft x rays, good agreement between experiment and simulation was also obtained for the temperature histories of thin tracer layers buried at different depths in the targets. This increases confidence in the modeling capability.

We are very grateful to the laser and target preparation staff at the Rutherford Appleton Laboratory for their considerable support and effort during the experiments. Also we thank M. Desselberger for useful discussions concerning the imaging system, B. Evans for manufacturing the multilayer coatings, J. Foster for the loan of the time-resolving photodiode and recording system, D. Kania for the loan of diamond photodetectors, and J. Hansom for valuable assistance with data analysis. This work was funded jointly by the SERC and MoD.

*Present address: Atomic Weapons Establishment, Aldermaston, United Kingdom.

†Present address: Lawrence Livermore National Laboratory, Livermore, CA 94550.

[1] See, for example, S. P. Obenschain *et al.*, Phys. Rev. Lett. **50**, 44 (1983).

[2] J. Edwards, M. Dunne, D. Riley, R. Taylor, O. Willi, and S. J. Rose, Phys. Rev. Lett. **67**, 3780 (1991).

[3] S. J. Davidson *et al.*, Appl. Phys. Lett. **52**, 847 (1988); R. Sigel *et al.*, Phys. Rev. Lett. **65**, 587 (1990); L. B. DaSilva *et al.*, Phys. Rev. Lett. **69**, 438 (1992).

[4] B. A. Remington *et al.*, Phys. Rev. Lett. **67**, 3259 (1991).

[5] J. Edwards *et al.*, in *Proceedings of the Sarasota Workshop on the Properties of Hot Dense Matter*, edited by W. Goldstein *et al.* (World Scientific, Singapore, 1991), p. 207.

[6] D. Kania *et al.*, Phys. Rev. A **46**, 7853 (1992).

[7] M. Desselberger, T. Afshar-rad, F. Khattak, S. Viana, and O. Willi, Appl. Opt. **30B**, 2285 (1991).

[8] J. P. Christiansen, D. E. T. F. Ashby, and K. V. Roberts, Comput. Phys. Commun. **7**, 271 (1974).

[9] J. Edwards, V. Barrow, O. Willi, and S. J. Rose, Europhys. Lett. **11**, 631 (1990).

[10] S. J. Rose, J. Phys. B **25**, 1667 (1992).

[11] J. Grun *et al.*, Phys. Rev. Lett. **58**, 2672 (1987).

[12] T. Endo, H. Shigara, K. Shihoyama, and Y. Kato, Phys. Rev. Lett. **60**, 1022 (1988).

[13] T. Endo, H. Shigara, and Y. Kato, Phys. Rev. A **42**, 918 (1990).

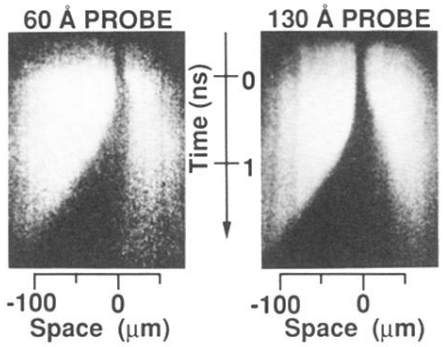

FIG. 1. Streaked radiograms of 2.8 μm CH foils heated by soft x rays for probe wavelengths of 130 and 60 Å. Drive incident from right.